Epitaxial integration and defect structure of layered-SnSe films on PbSe/III-V substrates

*Brian B. Haidet[1], Eamonn Hughes[1], Kunal Mukherjee[2],**

[1]Materials Department, University of California: Santa Barbara, Santa Barbara CA 93106, USA

[2]Department of Materials Science and Engineering, Stanford University, Stanford CA 94305, USA

kunalm@stanford.edu

ABSTRACT. We synthesize epitaxial films of SnSe, a van der Waals (vdW) layered semiconductor, on III-V substrates via molecular beam epitaxy. While direct deposition of SnSe on GaAs(001) surfaces results in polycrystalline growth, the structural similarity between the distorted-rocksalt SnSe and a rocksalt PbSe interlayer facilitates ordered quasi-vdW epitaxy of SnSe with only discrete in-plane rotations arising from the lower film symmetry. Towards manipulating the layering of SnSe for improved mechanical, optoelectronic, and ferroelastic/ferroelectric properties, we show SnSe/PbSe-on-III-V interfaces are structurally commensurate and chemically compatible enough for passage of sub-unit-cell surface steps and threading dislocations with partial Burgers vectors into the layered lattice from the 3D template. Such interfaces and extended defects results in novel stacking in SnSe along with the potential to crosslink layers across the vdW gap and yield films of mixed dimensionality. We assess the prospect of thermal expansion mismatch relief via sliding vdW interfaces in a 3D/layered/3D-bonded heterostructure using PbSe/SnSe/PbSe-on-InAs and find this to be ineffective against cracking as dislocation diffusion, grain boundaries, and crosslinking defects embrittle the heterostructure.

1. Introduction

Integrating semiconductors with dissimilar structural dimensionality and bonding in heterostructures enables harnessing new physical phenomena for devices.[1,2] A broad class of layered semiconductors with covalent intralayer bonding and van der Waals (vdW) interlayer bonding (hence, strongly bonded in the plane of the layers or in 2D) are being intensely investigated for their unique properties. When integrated with conventional semiconductor substrates like Si and III-V that are strongly bonded in 3D, these materials are generating significant excitement for a special class of layered-2D/3D heterostructures. Such mixed-dimensional heterostructures show promise for improved electronic devices, circumventing the limitations of lattice or thermal mismatch strain, as well as facilitating layer-transfer for substrate re-use.[3–7] Newer generations of semiconductor devices with unprecedented properties may emerge if we are able to manage dissimilarities in structure and bonding that constitute such a heterostructure. This requires an in-depth understanding of epitaxial synthesis and defect management in the integration of layered-2D with conventional 3D-bonded materials.

A common route to layered-2D/3D quasi-vdW integration relies on the hexagonal arrangement of atoms shared by many layered-2D transition metal dichalcogenides (TMDCs) and common 3D substrates, specifically the (0001) face of hexagonal materials like sapphire[8] and GaN, and the (111) face of cubic materials like GaAs and Si.[9,10] Yet, TMDCs represent only a subset of layered semiconductors and numerous lower symmetry materials remain underexplored. (100)-oriented SnSe is one such layered-2D semiconductor with a lower symmetry orthorhombic (Pnma) structure (a=11.50 Å, b=4.15 Å, c=4.45 Å), related to black phosphorus, that has been investigated intensely for thermoelectric, optoelectronic, photovoltaic, and battery applications[11–13], primarily via bulk crystals or polycrystalline or nanocrystalline morphologies. The unit cell of SnSe consists

of two mutually 180° rotated bilayers stacked with armchair and zigzag projections along the b- and c-axes (A-B stacking), yielding a distorted-rocksalt structure projection along the a-axis. The bilayer itself consists of strong polar covalent bonds between tin and selenium atoms. The bilayers attach to each other via a vdW interaction, although enhanced by the existence of a lone pair on each tin atom that extends into the void between the bilayers. Although the growth of SnSe down to the single bilayer limit is not the focus of this study, there is great interest in single and odd-numbered multilayer SnSe and related IV-monochalcogenides to harness the unique in-plane ferroelectricity along the armchair direction.[14–18]

Bulk crystals of SnSe prepared via melt-growth (Bridgman) are of exceptional structural quality but thin films are frequently deposited by low-temperature chemical bath deposition or low purity physical vapor deposition and exhibit poor morphology.[12] Recently, SnSe films with improved structural quality, judged by x-ray diffraction (XRD) rocking curve peak widths (~0.1–0.2° out-of-plane tilt mosaicity), have been synthesized by pulsed laser deposition (PLD) on ionic rocksalt NaCl and MgO insulating substrates.[19,20] At the same time, molecular beam epitaxy (MBE) growth of orthorhombic SnSe did not improve upon structural quality over PLD.[21] In this study by Nguyen et al., MBE growth on MgO substrate yielded multiple (100)-oriented films with varying in-plane rotation—one epitaxial alignment minimized lattice mismatch and another minimized symmetry mismatch. Epitaxial integration of SnSe with III-V semiconductors will require mediating both aspects at the same time, a task we accomplish in this work by using a rocksalt PbSe buffer layer. We describe this route to integrating (100)-oriented SnSe on the technologically relevant but highly mismatched (001)-face of GaAs and InAs by MBE, and uncover new modulations in layering with potentially important implications for the properties of these heterostructures.

2. Experimental Section

III-V layers were grown in a Veeco Gen-III MBE system and IV-VI layers were grown in a Riber Compact 21 MBE system. Semi-insulating epi-ready GaAs(001) wafers were loaded into the Gen-III system and the oxide layer was thermally desorbed. A thin layer (<100 nm) of homoepitaxial GaAs was grown, utilizing a standard gallium effusion cell and a cracked arsenic source. After the reflection high-energy electron diffraction (RHEED) pattern of the GaAs surface appeared smooth, growth was halted and the surface was capped with amorphous arsenic for out-of-vacuum transfer to the Compact 21 system.

The Compact 21 MBE is equipped for growth of IV-VI materials with solid PbSe and SnSe compound sources. After thermal desorption of the protective arsenic cap, exposure to PbSe flux at 400 °C transforms the GaAs (2×4) reconstructed-surface into a (2×1) reconstruction that we have previously shown acts as an excellent template for single-orientation cube-on-cube nucleation of PbSe at 330 °C.[22] A thin PbSe buffer was grown followed by deposition of SnSe at a substrate temperature of approximately 300 °C using molecular SnSe flux with a beam-equivalent pressure of approximately 3×10^{-7} Torr that corresponds to a growth rate of 0.4 Å/s. We use the same procedure to prepare heterostructures on InAs(001) wafers for the experiment on thermal expansion mismatch relief. As a point of comparison, we also deposited SnSe directly on GaAs(001) substrates without GaAs regrowth or a PbSe buffer. Such GaAs templates were loaded directly into the IV-VI MBE and the epi-ready oxide was desorbed under an Sb or Se overpressure.

Scanning electron microscopy (SEM) images were recorded on FEI Nova Nano, ThermoFisher Apreo C, and ThermoFisher Apreo S systems utilizing in-column secondary electron detectors. X-ray diffraction (XRD) experiments were performed on a Panalytical MRD PRO system. Samples were prepared for scanning transmission electron microscopy (STEM) via

a focused ion beam (FIB) lift-out process in an FEI Helios Dualbeam system. Cross-sectional STEM analysis was completed on a ThermoFisher Talos STEM, utilizing a bright field (BF) and a high-angle annular dark field (HAADF) detector. Electron channeling contrast imaging (ECCI) micrographs were recorded on the ThermoFisher Apreo C microscope utilizing an annular backscatter detector. The SnSe grain structure imaged by ECCI in Figure 3d was prepared via glancing angle FIB polishing.

3. Results and Discussion

A. Single orientation epitaxy of SnSe on GaAs (001)

We find growth of SnSe directly on on-axis GaAs(001) with its epi-ready oxide desorbed under Se or Sb overpressure results in many orientations of SnSe nuclei forming on the substrate surface, many of which have facets tilted out of the growth plane (Figure 1a-b) leading to poor film morphology. In the growth of the related material IV-VI material PbSe on GaAs(001), we have seen that a high temperature (400 °C) PbSe flux exposure (re-evaporating excess PbSe) helps create a template for subsequent low temperature (280–330 °C) ordered growth of PbSe on GaAs substrates.[22] The pre-treatment helps the epitaxial layer overcome the chemical and geometric changes between the zincblende and rocksalt structures. Directly adapting this method for the distorted-rocksalt SnSe does not work, as regrown GaAs surfaces that have been pre-treated with high temperature SnSe flux or PbSe flux still produce misoriented nuclei (Figure 1c-d), albeit growth on the PbSe flux-treated substrates is somewhat improved. In all these polycrystalline cases, the morphology suffers as orientation-dependent growth rates result in rough, faceted surfaces on the scale of hundreds of nanometers. Ultimately, we find that a finite-thickness interlayer of PbSe yields single out-of-plane orientation growth of SnSe on GaAs (Figure 1e),

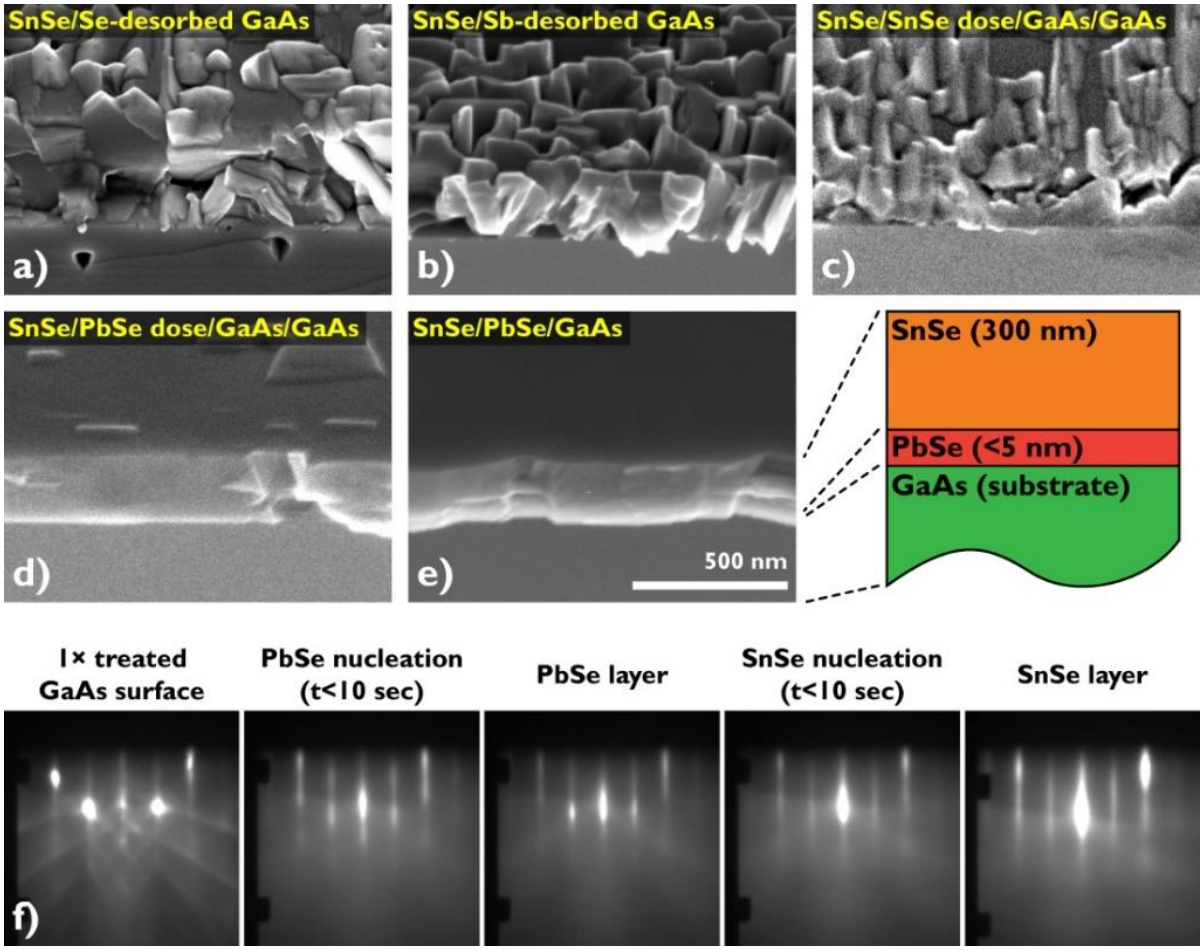

Figure 1. SEM images taken at 45° tilt near a GaAs{110} cleaved edge to observe the film's top surface and a limited cross section. Surfaces in (a) and (b) were prepared by desorbing the epi-ready oxide from GaAs wafers and immediately beginning SnSe growth, while surfaces in (c) and (d) were regrown GaAs surfaces treated with IV-VI flux at elevated temperature. The SnSe film in (e) was grown on top of a thin PbSe interlayer. The cleave on (e) is rougher because of the preferential {100} cleaving of the rocksalt PbSe film. Growing SnSe on a rocksalt PbSe (chemically similar and with 90° bond angles) template helps create a smoother film with fewer extra orientations. (f) shows RHEED patterns throughout nucleation and growth of the structure in (e).

requiring no special switching sequence between PbSe and SnSe. With this technique, we see very smooth transition from a streaky (1×1) rocksalt surface to a streaky (1×1) orthorhombic (distorted-rocksalt) surface in RHEED (Figure 1f). SnSe takes on a epitaxial arrangement on chemically- and structurally-compatible rocksalt PbSe, where SnSe[100] (a-axis) is parallel to PbSe[001], and SnSe[001] is parallel to either PbSe[110] or PbSe[$1\bar{1}0$]. With the 45° rotated in-plane orientation to the cubic unit cell of the template, SnSe is overall −4% and −11% mismatched to the GaAs lattice parameter at room temperature.

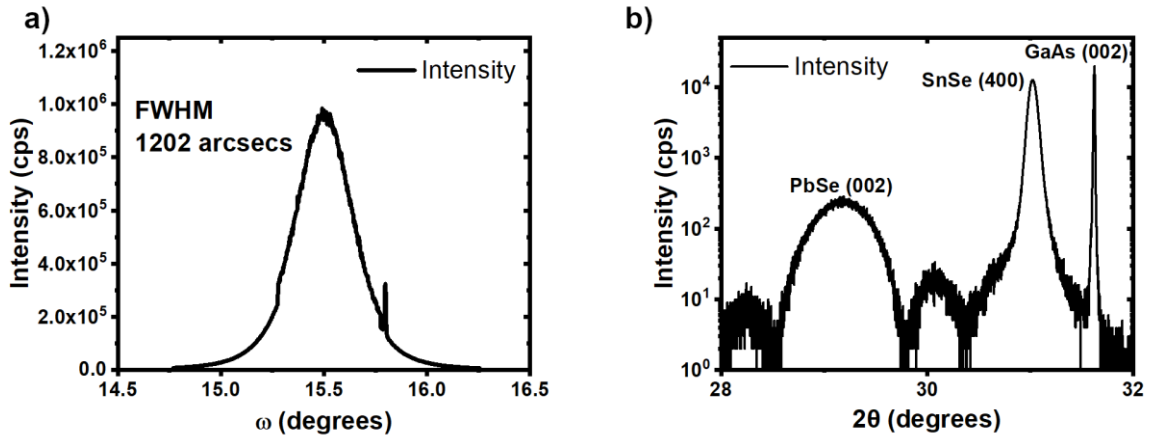

Figure 2. (a) Double-axis rocking curves of the (400) reflection of 250 nm SnSe on PbSe/GaAs. From Gaussian fitting of the peaks, FWHM of 0.33° is extracted. The small peaks/discontinuities at low intensity are due to the automatic x-ray beam attenuator activating and deactivating. (b) Triple-axis 2θ-ω scan of the SnSe (400) reflection. Also visible are the (002) peaks of the GaAs substrate and the PbSe interlayer with thickness fringes. An out-of-plane expansion of 0.17% along the a-axis, is measured for SnSe film. The PbSe interlayer is compressed 0.1% in the out-of-plane direction.

An obvious consequence of the large lattice-mismatch to GaAs is the dislocation content in the films. The starting PbSe-on GaAs template has a threading dislocation density of about $10^9/cm^2$ (see Figure 5), and this controls the growth mode of SnSe as we show subsequently. We measure an XRD rocking curve peak width of 0.33° for the (400) reflection on a 250 nm thick SnSe film on the PbSe-on-GaAs template (Figure 2a), with only a small 0.17% out-of-plane expansion along the a-axis measured from the 2θ-ω scan (Figure 2b), indicating that most of the lattice-mismatch strain is relaxed. We do not focus on the defect-mediated strain relaxation mechanism in SnSe in this work due to the exceedingly large initial mismatch and anisotropic thermal expansion mismatch between the films and the substrate that may be relieved using unconventional means such as incoherent interfaces in addition to localized misfit dislocations. In fact, a large part of the overall mismatch to GaAs may instead be relaxed at the PbSe/GaAs interface (≈ −8% mismatch), as the growth mode of the ultrathin PbSe is not layer-by-layer.

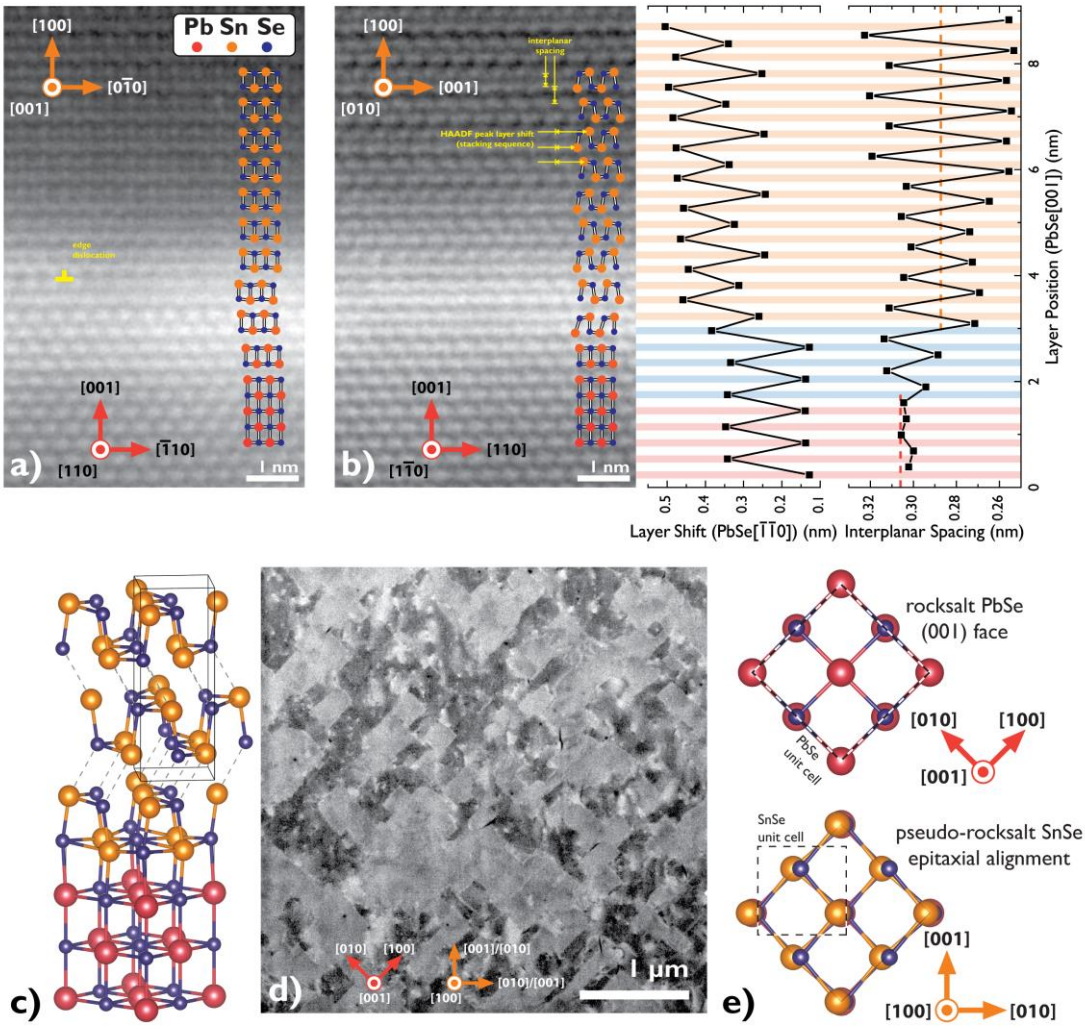

Figure 3. (a) and (b), orthogonal cross-sectional projections of the interface. [HAADF images processed with linear brightness/contrast and 0.2 Å gaussian blur.] (b) includes two graphs which, based on averaged HAADF contrast, show the lateral layer shift and interplanar spacing of and between each monolayer of atoms. The blue-marked region is transitionary and contains a layered structure with rocksalt-like stacking. (c) Isometric projection of a hypothetical sharp interface, conventional SnSe unit cell included. (d) ECCI of a SnSe layer polished by FIB showing two populations of 90° rotated grains with rectangular grain boundaries, and threading dislocation contrast within one of those populations of grains. (e) the pseudo-rocksalt stacking of SnSe on PbSe, showing the similarity of the PbSe (001) surface and the SnSe (100) surface. The SnSe unit cell shown has been slightly strained to appear square. Note that even in this symmetrized form, SnSe has lower rotational symmetry than PbSe.

Where an interface between PbSe and GaAs (chemically incompatible or immiscible 3D-bonded materials) or Bi_2Se_3/SiC (chemically incompatible or immiscible layered-2D/3D materials) may be atomically sharp[23], the chemically-compatible SnSe/PbSe interface we observe is distinctly smeared out over a few vdW bilayers shown in Figure 3a-b. Notably, the onset of vdW

layer formation appears to precede the full SnSe orthorhombic structure by three bilayers (Figure 3b), resulting in an epitaxially constrained transition region with a layered structure but a rocksalt stacking order. Even beyond this transition region, the layer spacing does not stabilize for approximately 3 nm into the SnSe layer. We do not think it is reasonable to define a specific truncation point for the SnSe unit cell; instead, the unique chemical and structural similarities between these otherwise distinct materials allow for a wide transition region where stable solid solutions of (Pb,Sn)Se exist in both the rocksalt and Pnma structures. Recent atom probe tomography on these films shows an interdiffused region between PbSe and SnSe approximately 5 nm wide.[24] Also noteworthy is that our rocksalt-PbSe template is insufficient to guide SnSe into the metastable rocksalt phase recently shown to be a topological crystalline insulator and prepared using vdW-Bi_2Se_3 interfaces.[25,26] Prior work on PbSe/SnSe superlattices show that it is possible to use PbSe to stabilize SnSe in a rocksalt structure below 1.5–2 SnSe bilayers but not beyond that.[27]

When considered together with the A-B stacking motif of the unit cell, a-axis SnSe could just as easily nucleate in any of the four ways in plane on the (001) face of PbSe. Figure 3d shows two distinct populations of large μm-sized grains taken using plan-view ECCI: 0°/180° and 90°/270° in-plane rotations, with grain boundaries falling preferentially along the SnSe[110] and SnSe[$1\bar{1}0$] directions. The unique grain structure points to strong faceting of the SnSe islands in the initial stages of growth. We note that only two populations of grains can be seen in ECCI, not four, because a 180° rotation of SnSe is equivalent to a vertical displacement of $a/2$, rendering them indistinguishable to this technique. One orientation set of grains is also close to an electron channeling condition (darker contrast), making threading dislocations visible only inside these grains as white dots with a density is close to $10^9/cm^2$. The other set of SnSe grains is not close to a channeling condition and appears as even gray contrast although we expect a similar density of

threading dislocations here as well. This overall epitaxial arrangement is set by the atomic arrangement of individual layers that closely resemble the rocksalt (001) plane (Figure 3e); the base of the SnSe unit cell when elastically strained +4.4% in the [010] direction and -2.5% in the [001] direction is made square and corresponds with the (001) plane of PbSe rotated 45°.

We find a 200 nm thick SnSe film on SI-GaAs with only the high temperature PbSe-dose (not interlayer) is p-type with a carrier concentration of $6.8\times10^{15}/cm^3$ and a mobility of 26 $cm^2/V\text{-}s$ at room temperature, determined using a Hall effect measurement with the van der Pauw method and ohmic contacts via diffused indium dots. It is difficult to isolate a carrier concentration and mobility for SnSe when a thick PbSe interlayer is used as the latter acts as a parasitic conduction pathway being heavily n-type ($>10^{18}/cm^3$) with reasonably high mobility. If we reduce the PbSe interlayer to just 2–3 nm thick, we measure a p-type carrier concentration of around $10^{16}/cm^3$ with a mobility of around 30 $cm^2/V\text{-}s$ in a 50 nm SnSe film. While the heterovalent III-V/IV-VI interface nearby could distort the true charge carrier concentration, the mobility is on par with other demonstrations of SnSe thin films on rocksalt substrates.[19,28]

B. Altered layer stacking by steps and dislocations

We find that the highly commensurate crystal structures and compatible chemistry between PbSe and SnSe result in unique extended defects when surface steps and threading dislocations replicate or translate from the substrate into the lower-symmetry SnSe film. Figure 4a is a scheme of layer stacking sequences in SnSe films biased by steps at the interface and spiral growth around dislocations. When nucleating SnSe on PbSe, symmetry considerations allow for the synthesis of defective stacking sequences when different rotations of SnSe nucleate on adjacent PbSe terraces and overgrow each other resulting in a locally random sequence of the four different possible layer

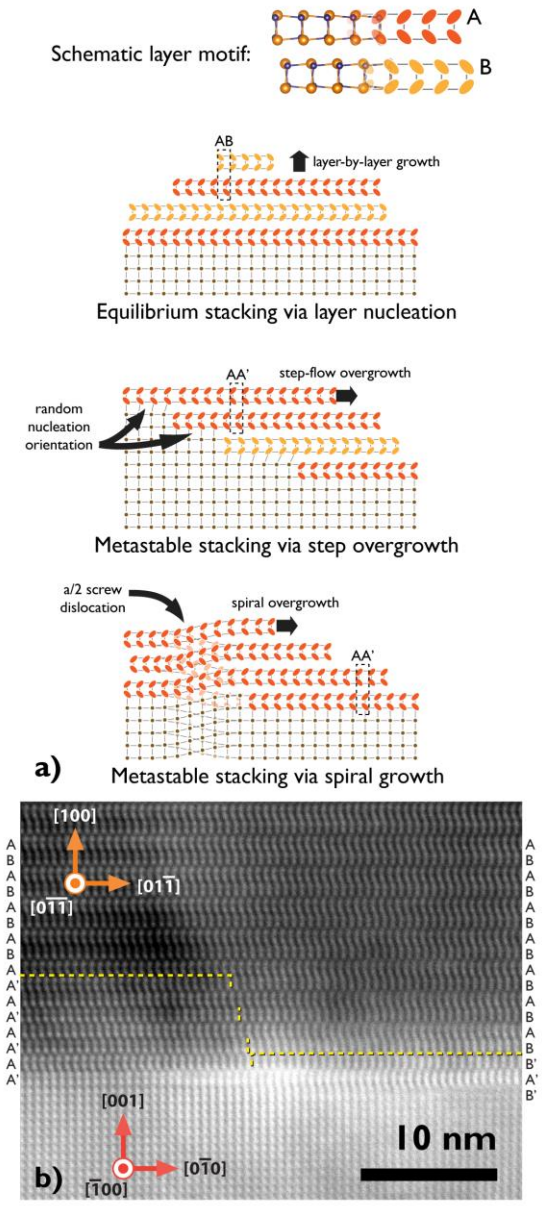

Figure 4. (a) Three ways to create different stacking sequences in SnSe viewed along the $[0\bar{1}\bar{1}]$ projection, the schematic motif above shows how one may distinguish the in-plane orientation by noting the relative alignment of the Sn and Se atoms. (b) PbSe[100] high resolution HAADF STEM cross section showing irregular stacking near the SnSe/PbSe interface (SnSe above PbSe). This projection cannot distinguish between the SnSe [011] and $[01\bar{1}]$ directions, which look identical, but can distinguish between these directions and their mirrors, $[0\bar{1}\bar{1}]$ and $[0\bar{1}1]$. Assuming that all layers pictured are either 0° or 180° rotated, boundaries between different stacking sequences A-A' and A-B are marked with a dotted line.

rotations mentioned previously. Figure 4b shows one sequence in our experiment where we term the stacking in the bottom left corner viewed along the SnSe $[0\bar{1}\bar{1}]$ projection as A-A' (note

corresponding $[\bar{1}00]$ projection of PbSe below based on the epitaxial relation). However, the film has an equilibrium A-B stacking on the right side of the image; the boundary between these domains only creates a defect in every other vdW layer and the overall 2D/layered nature of the material is preserved. After the SnSe in Figure 4b grows to be 10 nm thick, the equilibrium A-B stacking completely dominates, so the step-overgrowth or spiral growth effects which created the irregular A-A' stacking does not dominate epitaxy far from the interface. Related to the elusive A-A stacking observed in ultrathin SnS films on mica,[16] A-A' stacking comprises of bilayers that have the same direction of in-plane electric polarization but are laterally shifted with respect to each other (as opposed to pointing in opposite directions in A-B stacking) and should also give rise to macroscopic electric polarization. Without a STEM image along the armchair direction, we are unable to qualify whether the A-A' stacking we see here is the so-called A-C or A-E stacking described recently in SnS.[29] Regardless, these results motivate an investigation of the electrical properties of these unusually layered films when below 10 nm thickness.

Figures 5a-c show dislocations with a variety of Burgers vectors in the SnSe/PbSe/GaAs heterostructure, some of which appear replicated (copied) into SnSe directly from a thicker PbSe layer; note that the latter has a starting threading dislocation density exceeding $10^9/cm^2$ owing to the 8% lattice mismatch with GaAs. In analysis of a 22 μm wide STEM cross section, approximately one third of threading dislocations in the PbSe buffer layer have a matching dislocation directly above in the SnSe layer. The number of distinguishable defects (dislocations and grain boundaries) at the bottom of the SnSe layer is also about 25% higher than at the top of the PbSe buffer layer. However, many of these defects collide within the ~200 nm thick SnSe layer, leading to a modest (~25%) reduction of defects (including grain boundaries) at the film surface. This filtering does not appear to be complete, as several misfit dislocations are observed

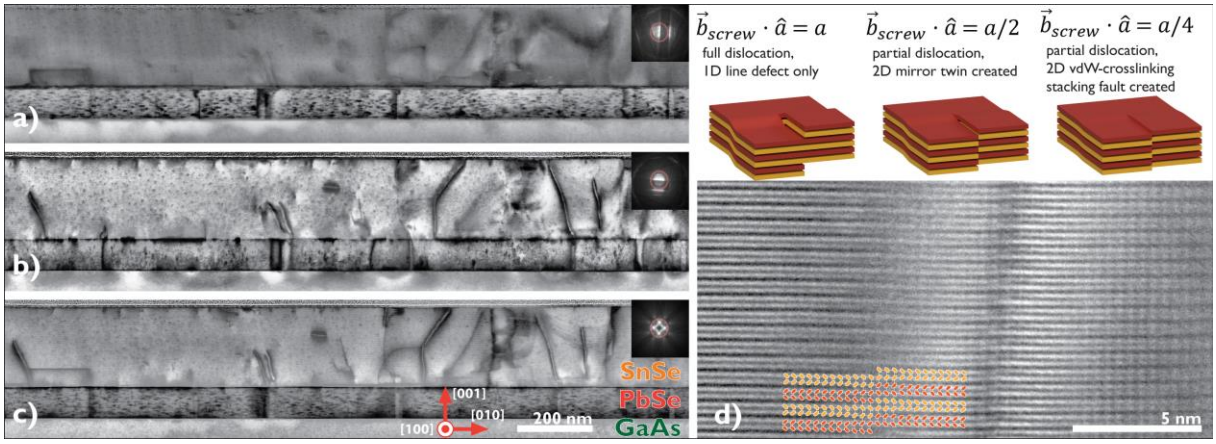

Figure 5. (a-c) Cross sectional STEM of a SnSe/PbSe/GaAs heterostructure with different diffraction conditions (diffraction patterns referenced to GaAs) to highlight that a mixture of Burgers vectors and stacking faults exist in these layers, (a) **g**=GaAs(040), (b) **g**=GaAs(004), (c) (100) zone. Note that the PbSe film has a cube on cube alignment to the substrate, but the SnSe film has unit cell axes rotated 45° in plane. This image is part of a larger analysis: across a 22 μm long STEM cross section, approximately 1/3 of dislocations in the PbSe buffer layer had a matching dislocation directly above in the SnSe layer, and the number of distinguishable defects (dislocations and grain boundaries) at the bottom of the SnSe layer is approximately 25% higher than at the top of the PbSe buffer layer. (d) (Upper) Scheme showing full 'a' dislocations and partial dislocations with 'a/2' and 'a/4' Burgers vectors bound different 2D stacking faults. (Lower) An 'a/4' stacking fault is pictured with HAADF STEM, demonstrating crosslinking between vdW sheets. [Processing notes: (a) enhanced with local contrast adjustment. (d) multiple image stacking and smoothed with a 0.1Å Gaussian blur]

in rows less than 20 nm from the top of the layer. We use two different STEM two-beam conditions: **g**=PbSe(040) (Fig. 5a) and **g**=PbSe(004) (Fig. 5b), and a multi-beam on-zone condition PbSe[100] (Fig. 5c) to differentiate between Burgers vectors of the dislocations. Dislocations that appear in Figure 5a and not in Figure 5b have Burgers vectors that lie in the growth plane. These are the inter-layer dislocations; the edge misfit dislocation marked in Figure 3a also meets this criterion. Dislocations which appear in Figure 5b have a finite Burgers vector projection in the SnSe[100] direction and mark the edge of a vdW layer (misfit dislocation) or a helical spiral of vdW layer (threading dislocation). A majority of the threading dislocations show this behavior.

If the threading dislocations exiting the top surface of the PbSe buffer have the typical rocksalt Burgers vector of $\frac{a}{2}\langle 110\rangle$ type with a magnitude of 4.33 Å, this Burgers vector necessarily distorts when translated into SnSe with its pseudo-rocksalt epitaxial arrangement, leaving behind an interfacial dislocation that contains the balance of the Burgers vector.[30] Within a bilayer,

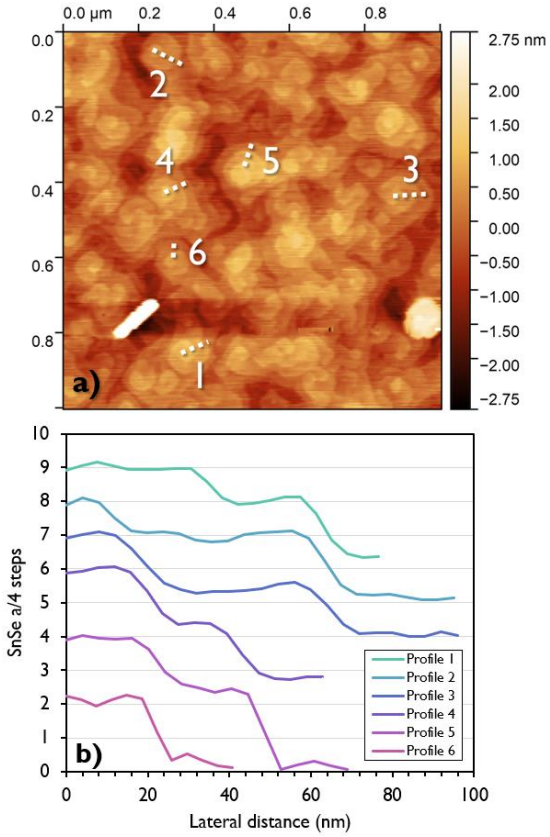

Figure 6. (a) AFM image showing the high density of spiral growth mounds on SnSe/PbSe-on-GaAs and indicating the location of profiles. (b) AFM height profiles measuring step heights surrounding regions of spiral growth. The first step in Profiles 1 and 2 are approximately one quarter the SnSe 'a' lattice parameter (a/4). These most likely arise from dislocations with Burgers vectors that are inherited from the underlying PbSe layer. The steps in Profiles 3 and 4 are somewhat ambiguous covering a height of approximately three quarter steps (3a/4) over two step changes. Profiles 5 and 6 are examples of 'a/2' steps.

Burgers vector magnitudes of 4.32 Å (Sn), or 3.96 Å (Se) are possible. Across bilayers, allowed Burgers vector magnitudes expand to 5.08 Å (Sn), 3.68 Å (Sn), 5.95 Å (Se), or 4.02 Å (Se). These are all lengths in an equilibrium unit cell and constitute only a partial dislocation in the [100]-oriented SnSe structure, that is half of a vdW bilayer or one quarter of a unit cell tall which we label '$a/4$' threading dislocations. We believe these dislocations are likely the most common form of substrate-inherited dislocation in these SnSe films and further reactions between these could produce '$a/2$' threading dislocations.

A perfect $'a'$ Burgers vector screw dislocation has a double bilayer step on the substrate and creates a line defect that preserves the crystalline structure of SnSe away from the core. These have been previously seen in plates and nanowires of SnS and GeS.[31] A partial $'a/2'$ dislocation has a single bilayer tall step on the substrate, and is expected to result in A-A type of stacking (including A-C, A-D, or A-E)[29] and the creation of a mirror twin *within* each vdW layer, discussed previously. Both these types of dislocations preserve the vdW gap, depicted schematically in Figure 5d (upper). However, dislocations inherited from the PbSe layer, with a '$a/4$' screw component, necessarily break the vdW gap and induce planar regions of crosslinking. The cross section of Figure 5d (lower) directly images a possible stacking fault that results from such a dislocation using HAADF STEM contrast. At this defect, alternate vdW layers are bonded together, locally creating a 3D covalently bonded network within SnSe (Figure 5d, upper scheme).

We may directly probe the screw-component of the Burgers vector of threading dislocations in SnSe by measuring the surface step height at growth spirals using AFM, shown in Figure 6a. The growth surface of SnSe is dominated by dislocation spirals, exceeding 10^9 cm^{-2} in density, a consequence of the high threading dislocation density of the PbSe/GaAs template. Unfortunately, this high density also results in significant overlap and interactions between the steps on the spirals and prevents unequivocal identification. We occasionally find spiral step heights very close to the center to be '$a/4$'-like after one turn of the screw, but they convert to '$a/2$' or '$3a/4$' step-heights further away from the center of the spiral. Several height traces are shown in Figure 6b showing these types of steps, tentatively supporting the existence of the threading dislocation caused defect seen in Fig. 5d.

Layered vdW materials frequently grow via spiral growth and step-flow mechanisms [32–36], implying a significant bias for adhesion at step edges and high adatom mobility on top of a vdW

sheet. A notable example of spiral growth in a vdW-bonded material comes from Liu at al.,[32] who grew Bi_2Se_3 on chemically incompatible graphene/SiC via 2D nucleation. They observe the standard 0.95 nm thick quintuple layers delaminating upwards to overgrow 0.26 nm surface steps on the substrate, creating new growth-plane dislocations and initiating spiral growth with a full $'a'$ screw dislocation (i.e. 1 quintuple layer spiral step height). A similar phenomenon of step overgrowth was studied in SnS growth over patterned layers of graphene that act as surface steps. Both single (0.32 nm) and double (0.67 nm) layer steps of graphene resulted in effectively '$a/2$' screw dislocations (i.e. 1 bilayer, 0.62 nm, spiral step height).[18] The tendency to form bilayers was again strong enough that vdW bilayers again folded up and over surface features, creating line defects, rather than breaking their own internal structure. Surprisingly, the '$a/2$' screw dislocation in SnS did not yield A-A or related stacking in the spiral, instead reverting to centrosymmetric A-B stacking when these spirals were characterized using TEM. The mechanism for this is unclear.[18] It appears that while Bi_2Se_3 or SnS could theoretically incorporate an unfavorable partial screw dislocation (fraction of a quintuple layer or bilayer, respectively), weak bonding to the substrate allows it to avoid this energetically costly outcome. We suggest that this opportunity is not available at the SnSe/PbSe interface, where a gradual transition in both chemistry and structure forces the epitaxial SnSe to incorporate defects like sub-unit-cell surface steps and '$a/4$' threading dislocations rather than overgrow them. Therefore, our work extends the idea of transmitting dislocations from a substrate for spiral growth of layered materials,[37] highlighting the potential for greater control and structural diversity via the judicious use of related or distorted crystal structures and partial dislocations.

The implications of these new layering defects and resulting change in symmetry on the electronic properties of SnSe remain to be characterized but there is good reason to expect new

properties. We have already mentioned the interest in A-A type stacking to realize robust low-dimensional ferroelectrics, and our work points to the possible use of dislocations from structurally nearly commensurate buffer layers to engineer this phase. Recently, twisting around screw dislocations with Burgers vectors corresponding to 'a' or multiple-'a' lengths in isostructural GeS nanowires was also shown to alter optical emission.[31,38] Finally, the dislocation content and grain boundary geometry is important also in thermal transport,[39] and SnSe epitaxial films with ordered grain boundaries and known dislocation structure may be important to expand on recent results in the field of thermoelectrics where polycrystalline SnSe films show great potential.[40]

C. SnSe as a mechanical interposer in thermal expansion strain relief

Epitaxial films present a unique opportunity to evaluate if layered-SnSe may act as a mechanical interposer to counteract the large thermal expansion mismatch between PbSe and III-V substrates, two 3D-bonded materials. To motivate this issue, we see that PbSe (001) films on InAs substrates routinely crack during cooldown if grown thicker than a few hundred nanometers due to a large thermal expansion mismatch (α_{PbSe}=19 ppm/K) with the substrate (α_{InAs}=4.5 ppm/K) coupled with an inactive primary and a sluggish secondary slip system of PbSe.[41] The ease with which vdW materials can slide over each other (effectively the glide of edge dislocations between the sheets) has historically made them attractive as mechanical lubricants and is claimed as a benefit of quasi-vdW epitaxy for integrating thermal-expansion-mismatched film and substrate[1,2,5,42]. Most quasi-vdW epitaxy is conducted with weakly interacting or incommensurate 2D-layered and 3D materials so the crystal quality of the 3D on 2D layer is anyway inferior, and prevents direct comparison to 3D/3D interfaces. The SnSe/PbSe/III-V system presents an

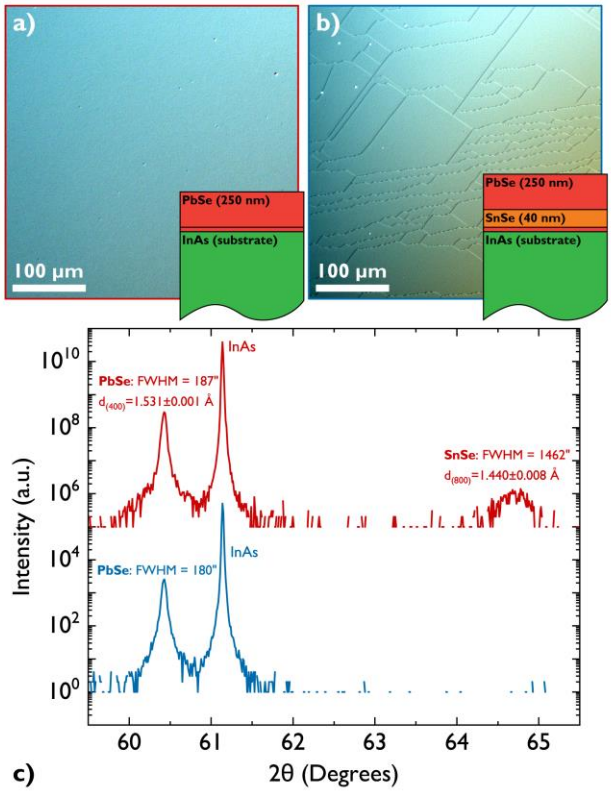

Figure 7. Optical Nomarski contrast images of (a) a 250 nm thick PbSe(001) epitaxial layer on an InAs(001) substrate and (b) the same thick layer, with 40 nm of SnSe epitaxial interposer between the PbSe nucleation layer and the 250 nm slab. The sample with the SnSe interposer exhibits surface cracking. (c) Triple-axis coupled 2θ-ω x-ray diffraction scans of the PbSe films from (a) and (b). Both PbSe films are of comparable quality showing potential for quasi-vdw epitaxy; the 40 nm SnSe interposer has significant tilt and variation in layer spacing.

intriguing contrast as we obtain PbSe films of comparable quality on SnSe templates as well as on III-V substrates. We evaluate if a SnSe interlayer allows for accommodation of this thermal expansion mismatch.

We grew two 250 nm thick PbSe films on InAs(001) substrates just below the critical thickness for cracking and supported one film on a 40 nm SnSe thermal strain relief layer. InAs is better lattice-matched to PbSe (−1.1%) and yields smoother surfaces that may be important for this experiment, but is otherwise identical in terms of growth conditions used for GaAs. Unexpectedly, optical Nomarski micrographs show the PbSe layer grown on SnSe/PbSe-on-InAs cracked while the PbSe grown directly on InAs did not (Figure 7 a-b). Further, the out-of-plane lattice parameter

measurements of PbSe in both instances are nearly identical (Figure 7c), indicating no additional relief of thermal strain. Thus, SnSe does not act as a strain relief layer but instead hastens the cracking process, transmitting thermal stresses efficiently from InAs to PbSe despite being a layered material and reducing the critical thickness for cracking in PbSe. The former effect may be ascribed to high interfacial toughness between SnSe bilayers, and we tentatively attribute the latter effect of embrittlement to alloy hardening of the secondary slip system facilitated by pipe diffusion of tin through threading dislocations in the PbSe layer.[24]

We may speculate as to why the bilayers of SnSe do not slide under shear stress imposed by thermal expansion mismatch. Bilayers of SnSe are harder to exfoliate from single crystals than graphene and other vdw-bonded TMDCs indicating stronger interlayer bonding, with some evidence of charge transfer between the layers.[43] In addition, we propose that extended defects that disrupt or crosslink the layered SnSe structure in our implementation may additionally inhibit sliding. In order for an edge misfit dislocation to glide across a perfect $'a'$ screw dislocation in SnSe, it must create a misfit dislocation segment, structurally appearing as a pair of extra half-planes terminating in the film, similar to structures investigated by Medlin et al. in Bi_2Se_3.[44] A similar process occurs when an in-plane edge dislocation glides through a $'a/2'$ screw dislocation where an energetically expensive mirror twin is enlarged, but the layered-structure is still not broken. Both these processes must be considered facile. In contrast, the numerous $'a/4'$ screw-component threading dislocations and rotational grain boundaries, which may include quarter-unit cell shifts, cross-link the vdW layers continuously over a large area and result in a mixed dimensional structure that no longer behaves mechanically like a layered material. A stacking fault like the one imaged in Figure 5d created by an $'a/4'$ screw dislocation would be a significant hurdle for a dislocation to cross: an edge misfit dislocation with its core between vdW bilayers

would glide through this stacking fault and find itself inside a single bilayer rather than between two. Breaking covalent bonds to glide or relying on climb to move into a new vdW channel are both slower.

Ideally then, a vdW bonded mechanical interposer should be: (1) highly symmetric to eliminate stacking faults or grain boundaries wherever possible, (2) weakly interacting with the substrate to retain integer-layer screw dislocations or steps, (3) strongly interacting with the desired epitaxial material to promote layer-by-layer nucleation for high crystal quality, and (4) patterned into small areas to allow for strain relief via free edges.[45] This tall order may be better met by layer transfer/wafer bonding methods over direct growth.

4. Conclusions

We harness the chemical and structural closeness of SnSe and PbSe and improve epitaxial uniformity of SnSe on III-V substrates in MBE, expanding the gamut of quasi-vdW 2D-layered/3D heterostructures. In addition to achieving large μm-size grains, judicious selection of the film and substrate also unlocks a route to introduce unconventional layering defects that may significantly alter the properties of the SnSe film, including the potential for inducing ferroelectricity and ferroelasticity. Such a method affords additional control and structural diversity over previous attempts to harness dislocations in nanostructured-layered materials based on precursor supersaturation control during synthesis. SnSe/PbSe-on-III-V thin films still retain rotational domains from symmetry mismatch, the removal of which require investigation of substrate miscut that could harness ledge-adatom attachment anisotropies in biasing one domain over another. Finally, our preliminary study touches upon the practical aspects of realizing a mixed-dimensional 3D/layered-2D/3D heterostructure, and highlights additional impediments to the prospect of

thermal expansion relief arising from high interfacial toughness in layered materials and low-symmetry crystal defects. The strength of film-substrate interactions in quasi-vdW epitaxy plays a dominant role in dictating the microstructure of the films and its resultant properties, a feature we must learn to control.

AUTHOR INFORMATION

Corresponding Author

Kunal Mukherjee, Department of Materials Science and Engineering, Stanford University, Stanford CA, 94305, USA. Email: kunalm@stanford.edu

Authors

Brian B. Haidet, Materials Department, University of California Santa Barbara, Santa Barbara, CA 93106, USA. Email: bbhaidet@ucsb.edu

Eamonn Hughes, Materials Department, University of California Santa Barbara, Santa Barbara, CA 93106, USA. Email: eamonnhughes@ucsb.edu

Author Contributions

The manuscript was written through contributions of all authors. All authors have given approval to the final version of the manuscript.

ACKNOWLEDGEMENTS

This work was supported through the National Science Foundation (NSF) CAREER award under grant No. DMR-1945321. We also acknowledge the use of shared facilities of the NSF MRSEC

at UC Santa Barbara, DMR 1720256. B.B.H. acknowledges support from the National Science Foundation Graduate Research Fellowship under grant No. 1650114. We acknowledge Jarod Meyer and Lillian Hughes for assistance with SnSe XRD and AFM measurements, and Kurt Olsson and John English for their MBE expertise and support.

Notes

The authors have no conflicts to disclose.

REFERENCES

(1) Bae, S.-H.; Kum, H.; Kong, W.; Kim, Y.; Choi, C.; Lee, B.; Lin, P.; Park, Y.; Kim, J. Integration of Bulk Materials with Two-Dimensional Materials for Physical Coupling and Applications. *Nat. Mater.* **2019**, *18* (6), 550–560. https://doi.org/10.1038/s41563-019-0335-2.

(2) Jariwala, D.; Marks, T. J.; Hersam, M. C. Mixed-Dimensional van Der Waals Heterostructures. *Nature Mater* **2017**, *16* (2), 170–181. https://doi.org/10.1038/nmat4703.

(3) Kim, J.; Bayram, C.; Park, H.; Cheng, C.-W.; Dimitrakopoulos, C.; Ott, J. A.; Reuter, K. B.; Bedell, S. W.; Sadana, D. K. Principle of Direct van Der Waals Epitaxy of Single-Crystalline Films on Epitaxial Graphene. *Nat Commun* **2014**, *5* (1), 4836. https://doi.org/10.1038/ncomms5836.

(4) Sarkar, D.; Xie, X.; Liu, W.; Cao, W.; Kang, J.; Gong, Y.; Kraemer, S.; Ajayan, P. M.; Banerjee, K. A Subthermionic Tunnel Field-Effect Transistor with an Atomically Thin Channel. *Nature* **2015**, *526* (7571), 91–95. https://doi.org/10.1038/nature15387.

(5) Alaskar, Y.; Arafin, S.; Lin, Q.; Wickramaratne, D.; McKay, J.; Norman, A. G.; Zhang, Z.; Yao, L.; Ding, F.; Zou, J.; Goorsky, M. S.; Lake, R. K.; Zurbuchen, M. A.; Wang, K. L. Theoretical and Experimental Study of Highly Textured GaAs on Silicon Using a Graphene Buffer Layer. *Journal of Crystal Growth* **2015**, *425*, 268–273. https://doi.org/10.1016/j.jcrysgro.2015.02.003.

(6) Ruzmetov, D.; Zhang, K.; Stan, G.; Kalanyan, B.; Bhimanapati, G. R.; Eichfeld, S. M.; Burke, R. A.; Shah, P. B.; O'Regan, T. P.; Crowne, F. J.; Birdwell, A. G.; Robinson, J. A.; Davydov, A. V.; Ivanov, T. G. Vertical 2D/3D Semiconductor Heterostructures Based on Epitaxial Molybdenum Disulfide and Gallium Nitride. *ACS Nano* **2016**, *10* (3), 3580–3588. https://doi.org/10.1021/acsnano.5b08008.

(7) Liu, C.; Huang, H.; Choi, W.; Kim, J.; Jung, K.; Sun, W.; Tansu, N.; Zhou, W.; Kuo, H.; Li, X. Hybrid Integration of N-MoS2/p-GaN Diodes by Quasi-van Der Waals Epitaxy. *ACS Appl. Electron. Mater.* **2020**, *2* (2), 419–425. https://doi.org/10.1021/acsaelm.9b00607.

(8) Zhang, X.; Choudhury, T. H.; Chubarov, M.; Xiang, Y.; Jariwala, B.; Zhang, F.; Alem, N.; Wang, G.-C.; Robinson, J. A.; Redwing, J. M. Diffusion-Controlled Epitaxy of Large

Area Coalesced WSe2 Monolayers on Sapphire. *Nano Lett.* **2018**, *18* (2), 1049–1056. https://doi.org/10.1021/acs.nanolett.7b04521.
(9) Mortelmans, W.; De Gendt, S.; Heyns, M.; Merckling, C. Epitaxy of 2D Chalcogenides: Aspects and Consequences of Weak van Der Waals Coupling. *Applied Materials Today* **2021**, *22*, 100975. https://doi.org/10.1016/j.apmt.2021.100975.
(10) Tarakina, N. V.; Schreyeck, S.; Borzenko, T.; Schumacher, C.; Karczewski, G.; Brunner, K.; Gould, C.; Buhmann, H.; Molenkamp, L. W. Comparative Study of the Microstructure of Bi2Se3 Thin Films Grown on Si(111) and InP(111) Substrates. *Crystal Growth & Design* **2012**, *12* (4), 1913–1918. https://doi.org/10.1021/cg201636g.
(11) Zhao, L.-D.; Lo, S.-H.; Zhang, Y.; Sun, H.; Tan, G.; Uher, C.; Wolverton, C.; Dravid, V. P.; Kanatzidis, M. G. Ultralow Thermal Conductivity and High Thermoelectric Figure of Merit in SnSe Crystals. *Nature* **2014**, *508* (7496), 373–377. https://doi.org/10.1038/nature13184.
(12) Shi, W.; Gao, M.; Wei, J.; Gao, J.; Fan, C.; Ashalley, E.; Li, H.; Wang, Z. Tin Selenide (SnSe): Growth, Properties, and Applications. *Advanced Science* **2018**, *5* (4). https://doi.org/10.1002/advs.201700602.
(13) Jhon, Y. I.; Lee, J.; Seo, M.; Lee, J. H.; Jhon, Y. M. Van Der Waals Layered Tin Selenide as Highly Nonlinear Ultrafast Saturable Absorber. *Advanced Optical Materials* **2019**, *7* (10), 1801745. https://doi.org/10.1002/adom.201801745.
(14) Wu, M.; Zeng, X. C. Intrinsic Ferroelasticity and/or Multiferroicity in Two-Dimensional Phosphorene and Phosphorene Analogues. *Nano Lett.* **2016**, *16* (5), 3236–3241. https://doi.org/10.1021/acs.nanolett.6b00726.
(15) Bao, Y.; Song, P.; Liu, Y.; Chen, Z.; Zhu, M.; Abdelwahab, I.; Su, J.; Fu, W.; Chi, X.; Yu, W.; Liu, W.; Zhao, X.; Xu, Q.-H.; Yang, M.; Loh, K. P. Gate-Tunable In-Plane Ferroelectricity in Few-Layer SnS. *Nano Lett.* **2019**, *19* (8), 5109–5117. https://doi.org/10.1021/acs.nanolett.9b01419.
(16) Higashitarumizu, N.; Kawamoto, H.; Lee, C.-J.; Lin, B.-H.; Chu, F.-H.; Yonemori, I.; Nishimura, T.; Wakabayashi, K.; Chang, W.-H.; Nagashio, K. Purely In-Plane Ferroelectricity in Monolayer SnS at Room Temperature. *Nat Commun* **2020**, *11* (1), 2428. https://doi.org/10.1038/s41467-020-16291-9.
(17) Chang, K.; Küster, F.; Miller, B. J.; Ji, J.-R.; Zhang, J.-L.; Sessi, P.; Barraza-Lopez, S.; Parkin, S. S. P. Microscopic Manipulation of Ferroelectric Domains in SnSe Monolayers at Room Temperature. *Nano Lett.* **2020**, *20* (9), 6590–6597. https://doi.org/10.1021/acs.nanolett.0c02357.
(18) Chang, Y.-R.; Higashitarumizu, N.; Kawamoto, H.; Chu, F.-H.; Lee, C.-J.; Nishimura, T.; Xiang, R.; Chang, W.-H.; Maruyama, S.; Nagashio, K. Atomic-Step-Induced Screw-Dislocation-Driven Spiral Growth of SnS. *Chem. Mater.* **2021**, *33* (1), 186–194. https://doi.org/10.1021/acs.chemmater.0c03184.
(19) Inoue, T.; Hiramatsu, H.; Hosono, H.; Kamiya, T. Heteroepitaxial Growth of SnSe Films by Pulsed Laser Deposition Using Se-Rich Targets. *Journal of Applied Physics* **2015**, *118* (20), 205302. https://doi.org/10.1063/1.4936202.
(20) Hou, S.; Li, Z.; Xue, Y.; Ning, X.; Wang, J.; Wang, S. Surprisingly High In-Plane Thermoelectric Performance in a-Axis-Oriented Epitaxial SnSe Thin Films. *Materials Today Physics* **2021**, *18*, 100399. https://doi.org/10.1016/j.mtphys.2021.100399.
(21) Nguyen, V. Q.; Duong, V. T.; Nguyen, T. H.; Kang, R.; Pham, A. T.; Tran, V. T.; Nguyen, C. K.; Duong, A. T.; Phan, T. B.; Kim, J.; Cho, S. Se/Sn Flux Ratio Effects on

Epitaxial SnSe Thin Films; Crystallinity & Domain Rotation. *Journal of Alloys and Compounds* **2020**, *840*, 155680. https://doi.org/10.1016/j.jallcom.2020.155680.
(22) Haidet, B. B.; Hughes, E. T.; Mukherjee, K. Nucleation Control and Interface Structure of Rocksalt PbSe on (001) Zincblende III-V Surfaces. *Physical Review Materials* **2020**, *4* (3), 033402. https://doi.org/10.1103/PhysRevMaterials.4.033402.
(23) Kepaptsoglou, D. M.; Gilks, D.; Lari, L.; Ramasse, Q. M.; Galindo, P.; Weinert, M.; Li, L.; Nicotra, G.; Lazarov, V. K. STEM and EELS Study of the Graphene/Bi2Se3 Interface. *Microscopy and Microanalysis* **2015**, *21* (S3), 1151–1152. https://doi.org/10.1017/S1431927615006546.
(24) Hughes, E. T.; Haidet, B. B.; Bonef, B.; Cai, W.; Mukherjee, K. Pipe-Diffusion-Enriched Dislocations and Interfaces in SnSe/PbSe Heterostructures. *Phys. Rev. Materials* **2021**, *5* (7), 073402. https://doi.org/10.1103/PhysRevMaterials.5.073402.
(25) Wang Zhenyu; Wang Jianfeng; Zang Yunyi; Zhang Qinghua; Shi Jin-An; Jiang Tian; Gong Yan; Song Can-Li; Ji Shuai-Hua; Wang Li-Li; Gu Lin; He Ke; Duan Wenhui; Ma Xucun; Chen Xi; Xue Qi-Kun. Molecular Beam Epitaxy-Grown SnSe in the Rock-Salt Structure: An Artificial Topological Crystalline Insulator Material. *Advanced Materials* **2015**, *27* (28), 4150–4154. https://doi.org/10.1002/adma.201501676.
(26) Jin, W.; Vishwanath, S.; Liu, J.; Kong, L.; Lou, R.; Dai, Z.; Sadowski, J. T.; Liu, X.; Lien, H.-H.; Chaney, A.; Han, Y.; Cao, M.; Ma, J.; Qian, T.; Wang, S.; Dobrowolska, M.; Furdyna, J.; Muller, D. A.; Pohl, K.; Ding, H.; Dadap, J. I.; Xing, H. G.; Osgood, R. M. Electronic Structure of the Metastable Epitaxial Rock-Salt SnSe {111 } Topological Crystalline Insulator. *Physical Review X* **2017**, *7*, 041020. https://doi.org/10.1103/PhysRevX.7.041020.
(27) Hiroi, Z. Thickness-Dependent Structural Transformation in PbSe-SnSe Artificial Superlattice. *Philosophical Magazine B* **1990**, *61* (5), 895–925. https://doi.org/10.1080/13642819008207570.
(28) Inoue, T.; Hiramatsu, H.; Hosono, H.; Kamiya, T. Nonequilibrium Rock-Salt-Type Pb-Doped SnSe with High Carrier Mobilities ≈ 300 Cm2/(Vs). *Chem. Mater.* **2016**, *28* (7), 2278–2286. https://doi.org/10.1021/acs.chemmater.6b00307.
(29) Yonemori, I.; Dutta, S.; Nagashio, K.; Wakabayashi, K. Thickness-Dependent Raman Active Modes of SnS Thin Films. *AIP Advances* **2021**, *11* (9), 095106. https://doi.org/10.1063/5.0062857.
(30) Aindow, M. On the Extension of Substrate Dislocations into Heteroepitaxial Deposits. *Philosophical Magazine Letters* **1990**, *62* (3), 139–141. https://doi.org/10.1080/09500839008215050.
(31) Sutter, P.; Wimer, S.; Sutter, E. Chiral Twisted van Der Waals Nanowires. *Nature* **2019**, *570* (7761), 354–357. https://doi.org/10.1038/s41586-019-1147-x.
(32) Liu, Y.; Weinert, M.; Li, L. Spiral Growth without Dislocations: Molecular Beam Epitaxy of the Topological Insulator Bi 2Se 3 on Epitaxial Graphene/SiC(0001). *Physical Review Letters* **2012**, *108* (11), 1–5. https://doi.org/10.1103/PhysRevLett.108.115501.
(33) Liu, J.; Huang, Q.; Qian, Y.; Huang, Z.; Lai, F.; Lin, L.; Guo, M.; Zheng, W.; Qu, Y. Screw Dislocation-Driven Growth of the Layered Spiral-Type SnSe Nanoplates. *Crystal Growth and Design* **2016**, *16* (4), 2052–2056. https://doi.org/10.1021/acs.cgd.5b01708.
(34) Nie, Y.; Barton, A. T.; Addou, R.; Zheng, Y.; Walsh, L. A.; Eichfeld, S. M.; Yue, R.; Cormier, C. R.; Zhang, C.; Wang, Q.; Liang, C.; Robinson, J. A.; Kim, M.; Vandenberghe, W.; Colombo, L.; Cha, P.-R.; Wallace, R. M.; Hinkle, C. L.; Cho, K. Dislocation Driven

Spiral and Non-Spiral Growth in Layered Chalcogenides. *Nanoscale* **2018**, *10* (31), 15023–15034. https://doi.org/10.1039/C8NR02280A.
(35) Liu, X.; Chen, Y. P.; Smith, D. J.; Zhang, Y.-H.; Liu, C.; Hasan, M. Z.; Dobrowolska, M.; Furdyna, J. K.; Fan, J.; Cao, H.; Wu, T.-L.; Pimpinella, R. E. MBE Growth of Thin Hexagonal Films Bi 2 Te 3 , Bi 2 Se 3 , and Their Alloys on Cubic GaAs (001) Substrates. In *Bismuth-Containing Compounds*; Li, H., Wang, Z. M., Eds.; Springer: New York, 2013; pp 263–279.
(36) Chen, R.; Cao, J.; Gee, S.; Liu, Y.; Yao, J. Growth and Properties of Dislocated Two-Dimensional Layered Materials. *MRS Advances* **2020**, *5* (64), 3437–3452. https://doi.org/10.1557/adv.2020.334.
(37) Morin, S. A.; Jin, S. Screw Dislocation-Driven Epitaxial Solution Growth of ZnO Nanowires Seeded by Dislocations in GaN Substrates. *Nano Lett.* **2010**, *10* (9), 3459–3463. https://doi.org/10.1021/nl1015409.
(38) Liu, Y.; Wang, J.; Kim, S.; Sun, H.; Yang, F.; Fang, Z.; Tamura, N.; Zhang, R.; Song, X.; Wen, J.; Xu, B. Z.; Wang, M.; Lin, S.; Yu, Q.; Tom, K. B.; Deng, Y.; Turner, J.; Chan, E.; Jin, D.; Ritchie, R. O.; Minor, A. M.; Chrzan, D. C.; Scott, M. C.; Yao, J. Helical van Der Waals Crystals with Discretized Eshelby Twist. *Nature* **2019**, *570* (7761), 358–362. https://doi.org/10.1038/s41586-019-1308-y.
(39) Cheng, Y.; Nomura, M.; Volz, S.; Xiong, S. Phonon–Dislocation Interaction and Its Impact on Thermal Conductivity. *Journal of Applied Physics* **2021**, *130* (4), 040902. https://doi.org/10.1063/5.0054078.
(40) Zhou, C.; Lee, Y. K.; Yu, Y.; Byun, S.; Luo, Z.-Z.; Lee, H.; Ge, B.; Lee, Y.-L.; Chen, X.; Lee, J. Y.; Cojocaru-Mirédin, O.; Chang, H.; Im, J.; Cho, S.-P.; Wuttig, M.; Dravid, V. P.; Kanatzidis, M. G.; Chung, I. Polycrystalline SnSe with a Thermoelectric Figure of Merit Greater than the Single Crystal. *Nat. Mater.* **2021**, 1–7. https://doi.org/10.1038/s41563-021-01064-6.
(41) Müller, P.; Fach, A.; John, J.; Tiwari, A. N.; Zogg, H.; Kostorz, G. Structure of Epitaxial PbSe Grown on Si(111) and Si(100) without a Fluoride Buffer Layer. *Journal of Applied Physics* **1996**, *79* (4), 1911–1916. https://doi.org/10.1063/1.361076.
(42) Koma, A. Van Der Waals Epitaxy—a New Epitaxial Growth Method for a Highly Lattice-Mismatched System. *Thin Solid Films* **1992**, *216* (1), 72–76. https://doi.org/10.1016/0040-6090(92)90872-9.
(43) Song, H.-Y.; Lü, J.-T. Density Functional Theory Study of Inter-Layer Coupling in Bulk Tin Selenide. *Chemical Physics Letters* **2018**, *695*, 200–204. https://doi.org/10.1016/j.cplett.2018.02.013.
(44) Medlin, D. L.; Erickson, K. J.; Limmer, S. J.; Yelton, W. G.; Siegal, M. P. Dissociated 1/3<0-111> Dislocations in Bi2Te3 and Their Relationship to Seven-Layer Bi3Te4 Defects. *J Mater Sci* **2014**, *49* (11), 3970–3979. https://doi.org/10.1007/s10853-014-8035-4.
(45) Yu, H.-H.; He, M. Y.; Hutchinson, J. W. Edge Effects in Thin Film Delamination. *Acta Materialia* **2001**, *49* (1), 93–107. https://doi.org/10.1016/S1359-6454(00)00293-7.

'For Table of Contents Use Only'

Epitaxial integration and defect structure of layered-SnSe films on PbSe/III-V substrates

Brian B. Haidet, Eamonn Hughes, Kunal Mukherjee

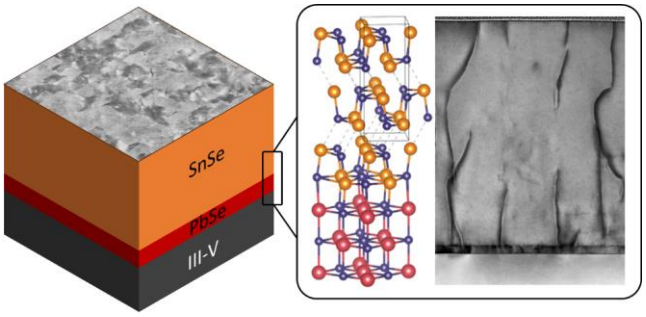

Synopsis:

Epitaxial films of (100)-oriented SnSe are grown on GaAs (001) substrates using a thin PbSe interlayer. The chemical and structural closeness of the orthorhombic SnSe and rocksalt PbSe enable micron-sized grains but also facilitate the passage of sub-unit-cell height structural defects of steps and threading dislocations. These potentially affect layering in SnSe and its electronic and mechanical properties.